Macromolecules

pubs.acs.org/Macromolecules Article

Effect of Host Incompatibility and Polarity Contrast on Ion Transport in Ternary Polymer-Polymer-Salt Blend Electrolytes

Bill K. Wheatle, Nathaniel A. Lynd, and Venkat Ganesan*

Cite This: *Macromolecules* 2020, 53, 875−884 Read Online

ACCESS | Metrics & More | Article Recommendations | Supporting Information

ABSTRACT: We study ternary polymer-polymer-salt blend electrolytes using coarse-grained molecular dynamics. We specifically examine the influence of the polymer hosts' incompatibility and polarity contrast on electrolyte ion transport characteristics. We find that, at moderate- to high-polarity contrasts, improving the miscibility of the polymer hosts by reducing their inherent incompatibility improves ionic transport, as measured by the ionic conductivity. However, contrary to expectations, ionic conduction slows with increased miscibility in low-polarity contrast electrolytes. Upon examining the underlying material properties, we find that ionic aggregation exhibits trends similar to ionic conductivity and is thus likely the controlling factor in these polymer-blend electrolytes. Our results suggest that ionic conduction can be improved in real polymer electrolytes by choosing chemistries that promote simultaneous miscibility and polarity contrast between the polymer hosts.

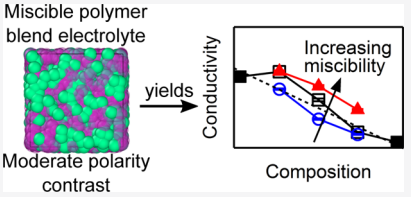

INTRODUCTION

Lithium-ion batteries (LIBs) are electrochemical devices that can reversibly store and discharge energy by shuttling lithium. They have found application in many consumer products, such as laptops, cell phones, and electric vehicles, owing to their high cyclabilities, energy densities, and power densities.[1] The electrolytes in LIBs are ionically conducting yet electronically insulating materials sandwiched between their electrodes. This combination of properties inhibits LIB self-discharge when disconnected from a load while enabling facile charge transport during charge/discharge cycles.

Facile ionic transport, as measured in part by the ionic conductivity, is enabled by an electrolyte host which has fast innate dynamics and can solvate lithium ions well. Fast dynamics is typically promoted through the choice of a low-viscosity liquid host, such as dimethoxyethane, dimethyl carbonate, or diethyl carbonate, whose properties presumably arise from weak polar intermolecular interactions.[2,3] These weak interactions, characterized by a low dielectric constant, lead to a reduced propensity to solvate ions.[4] Thus, the second need for a high-performance electrolyte is often met by the addition of a highly polar solvent, such as ethylene carbonate.[2,3] These resultant blend small-molecule electrolytes (SMEs) have high ionic conductivities, thereby reducing the overpotential needed to drive ion transport.[2]

Interestingly, blends of SMEs have been found to have ionic conductivities higher than those of their correspondent pure electrolytes (electrolytes containing only one host), typically maximizing at some intermediate electrolyte composition.[2] At a molecular level, such observations have been rationalized by suggesting lithium ion's solvation shell consisting predominantly of the high-polarity component and largely excludes the high-mobility component.[5] The lithium ions then hop from shell to shell or diffuse with their solvation shells through a medium that consists predominantly of the high-mobility component.[2,5] This combination yields a unique environment, characterized by both fast dynamics and high ionic solvation strength, around a lithium ion that cannot be found in their pure electrolyte counterparts. Such a synergy on the molecular scale highlights the necessity of the blend SMEs being miscible, as the conduction mechanism through a demixed SME may be some simple average of the native conduction mechanisms of the high-mobility and high-polarity component electrolytes.[6]

Despite their success, SMEs bring with them several undesirable properties, such as flammability, electrochemical instability, and the additional need for mechanical support. These downsides could be mediated by replacing the liquid hosts with polar polymers. However, it has been shown that polymers exchange their improved thermal, electrochemical, and mechanical stabilities for poor ionic transport[7] because of a combination of poor ionic solvation[8−12] and slow dynamics.[13−20]

Using blend SMEs as inspiration, we hypothesize that blending two polar polymers, one of which has fast dynamics and the other high polarities, may be a viable strategy to improve the ionic conductivity of polymer-based electrolytes (PBEs). We expect that these blend PBEs will exhibit similar positive deviations relative to the linear mixing rule seen in blend SMEs while still maintaining their desired chemical and mechanical robustness. However, as has been highlighted

Received: November 27, 2019
Revised: January 7, 2020
Published: January 21, 2020

https://dx.doi.org/10.1021/acs.macromol.9b02510
Macromolecules 2020, 53, 875−884

above, to gain the synergistic benefit of combining two polymer hosts, the resulting blend PBE should be miscible. As enthalpic self-interactions of one polymer tend to be favored over cross-interactions with other polymers, a blend of any two polymers is unlikely to be miscible at sufficiently high molecular weight.[21] Such incompatibility could be remedied through the inclusion of associative groups between polymers, such as hydrogen bonding moieties dispersed along the polymer chain.[22] In addition, Wang has interestingly shown that the addition of salt into polymer blends can improve their miscibility if they have large differences in their dielectric constants.[23]

The abovementioned considerations have inspired us to understand the roles of incompatibility and dielectric contrast on ion transport in blend PBEs. We believe that the inherent incompatibility of the host polymers and the polarity contrast between the hosts will strongly influence the conductivity of their resultant blend PBEs. In particular, we anticipate that large contrast between the polymer host dynamics and polarities will best improve ionic conductivity relative to that of the pure electrolytes. However, we further anticipate that such improvements can only be accessed in miscible blends, in which ions are well solvated by the high-polarity polymer but can diffuse through a medium whose dynamics are dominated by the high-mobility polymer.

We recognize the challenge of exploring the roles of incompatibility and dielectric contrast on ionic transport from an atomistic perspective, as we would need to identify chemistries that would to independently span a wide range in polarity contrast and host incompatibility. Instead, in this study, we use a molecular dynamics framework in combination with the so-called Stockmayer model. It is a simple coarse-grained model of polar fluids that allows us to easily vary the polarity of the high-mobility (denoted A) and high-polarity (denoted B) polymer components by varying the strength of a freely rotating, point electric dipole moment embedded in each repeat unit (RU) of each polymer.[24,25] Similar models have been previously employed to explore chain conformations of dilute polymers in solvent,[26,27] the competition between ionic aggregation and polymer dynamics and their relation to ion transport,[10] the effect of molecular weight and salt concentration on ion transport,[28] and the influence of molecular weight and chain connectivity on ion solvation[29−31] in polymer electrolytes. In a blend of weakly interacting Stockmayer polymers, Kumar and co-workers have shown that increasing the contrast in polymer polarity strongly decreases their solubility.[32,33] Such an increased phase separation tendency can be remedied by changing the polymer components. The Lennard-Jones cross-interaction parameter ε_{AB} is relative to their self-interaction parameters (ε_{AA}, ε_{BB}), both of which are set to 1.0 k_BT. Grest and co-workers found that blend incompatibility could be reduced when $\varepsilon_{AB}/(k_BT)$ decreased below 1.0.[34] We use the flexibility afforded by the independent nature of the cross-interaction parameter to tune the miscibility independent of the polarity contrast.

The remainder of this article is as follows: we describe in more detail the simulation method and parameters used in the Simulation Details section. In the Results and Discussion section, we present the variation of PBE miscibility and the environment around ions as a function of simulation parameters and relate them to measurements of their ionic conductivities. We combine insights from these measurements to ascertain the role of ionic aggregation and polymer dynamics in these blend electrolytes at the end of the Results and Discussion section. We conclude with recommendations for ideal-blend PBEs.

Simulation Details. As described in the introduction, the Stockmayer model is a coarse-grained model of polar fluids. Each polar molecule is represented by a bead in which is embedded a freely rotating, point electric dipole. This dipole can then interact with ions placed in the system, thus serving as a means to screen ion−ion interactions.[10,24,25,29−31]

As is commonly done in coarse-grained molecular dynamics, we represent all parameters in Lennard-Jones (LJ) units, the values of which are nondimensionalized by the following fundamental parameters: the characteristic mass $m = 2.99 \times 10^{-26}$ kg, the characteristic energy $\varepsilon = 5.27 \times 10^{-21}$ J, and the characteristic length $\sigma = 4.5$ Å.[31] In all simulations, we set the temperature $T^* = \frac{k_BT}{\varepsilon} = 1.0$, where k_B is the Boltzmann constant, and the mass of all particles to $m_i = m$, and note that the characteristic timescale $\tau = \left(\frac{m\sigma^2}{\varepsilon}\right)^{1/2} = 1.1$ ns. We represent the fundamental charge e in LJ units according to the following equation

$$e^* = \frac{e}{(4\pi\epsilon_0\sigma\varepsilon)^{1/2}} = 9.863 \tag{1}$$

where ϵ_0 is the permittivity of free space. Further, we represent the dipole strength of a poly(ethylene oxide) (PEO) RU at 373 K (1.7 D[10]) as μ_{EO}, according to the following equation

$$\mu_{EO} = \frac{(1.7\ D)(3.33564 \times 10^{-30}\ \mathrm{cm}/D)}{(4\pi\epsilon_0\sigma^3\varepsilon)^{1/2}} = 0.775 \tag{2}$$

For convenience, we express all dipole strengths as a multiple of μ_{EO}.

All systems consist of four types of particles: low-polarity monomer (denoted A), high-polarity monomer (B), anions (a), and cations (c). Point dipoles were embedded in beads of type A and B, whereas point charges were assigned to both the anions and cations. The dipole strength associated with A is 1.25 μ_{EO}, whereas $\Delta\mu = \mu_B - \mu_A = [0.1, 0.4, 0.8]\ \mu_{EO}$. Increasing a given polymer's polarity improves its solvation strength while slowing dynamics.[9,10,28] Thus, these values were chosen such that A poorly solvates ions but has fast dynamics and that B has similar solvation strength and dynamics as A at low $\Delta\mu$ and strong solvation strength and poor dynamics at high $\Delta\mu$.[10] We set the charges assigned to cations and anions to be $q_c = -q_a = e^*$ in all simulations.

All particles interacted through a mixture of nonbonded and bonded potentials. The nonbonded potential between particles i and j was of the following form

$$E_{ij}(r_{ij}) = E_{WCA}(r_{ij}) + E_{el}(r_{ij}) \tag{3}$$

where r_{ij} is the distance between particles i and j, and E_{el} is an electrostatic potential. As mentioned above, E_{WCA} denotes the Weeks−Chandler−Anderson potential[35]

$$E_{WCA}(r_{ij}) = 4\varepsilon_{ij}\left[\left(\frac{\sigma_{ij}}{r_{ij}}\right)^{12} - \left(\frac{\sigma_{ij}}{r_{ij}}\right)^{6} + \frac{1}{4}\right], \qquad r_{ij} \le 2^{1/6}\sigma_{ij} \tag{4}$$

Here, σ_{ij} and ε_{ij} are the LJ energy and radius. Because of the cutoff at $2^{1/6}\ \sigma_{ij}$, this potential simulates a purely repulsive interaction between all particles in the system. σ_{ij} is determined

https://dx.doi.org/10.1021/acs.macromol.9b02510
Macromolecules 2020, 53, 875−884

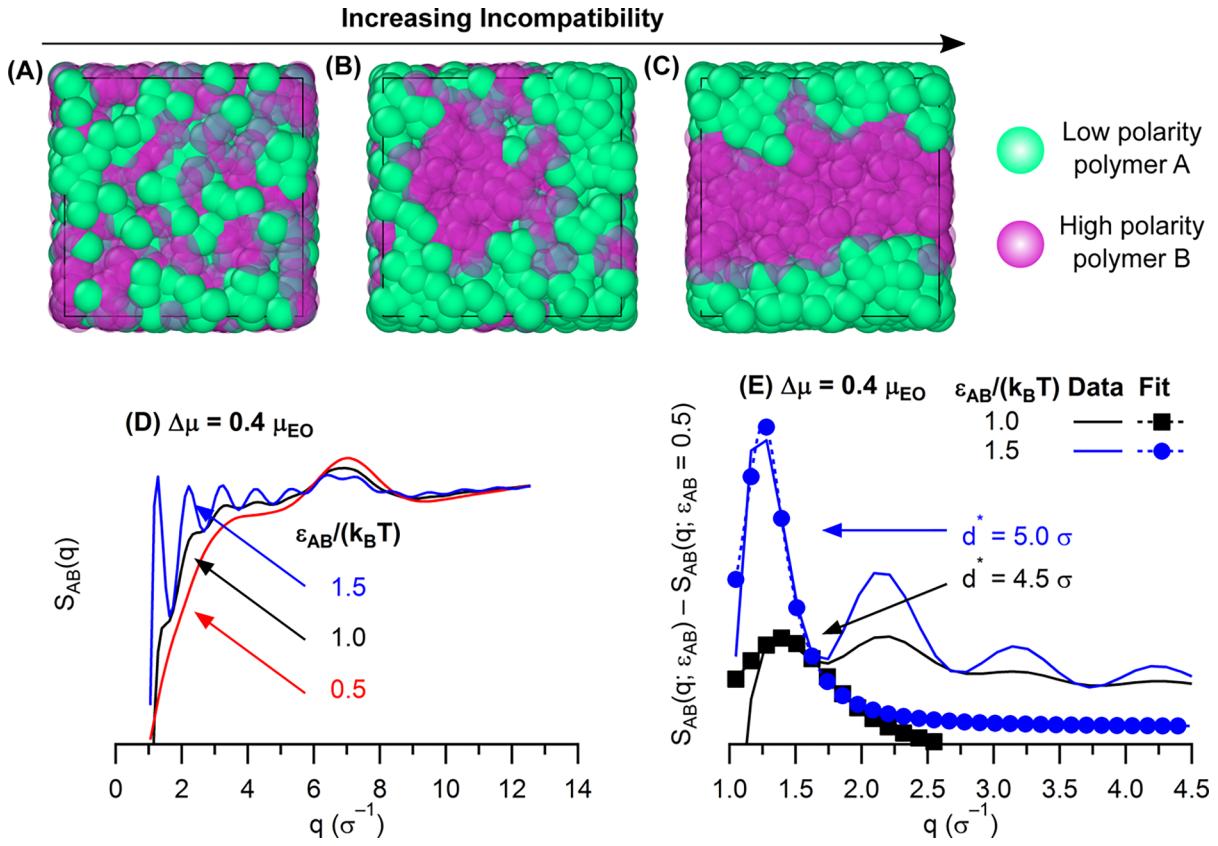

Figure 1. Simulation snapshots of the polymer hosts the $\Delta\mu/\mu_{EO} = 0.4$ blend electrolytes with incompatibility strengths $\varepsilon_{AB}/(k_BT)$ of (A) 0.5, (B) 1.0, and (C) 1.5. Light blue and purple particles correspond to A and B polymers, respectively. The blends more strongly phase segregate with increasing incompatibility. (D) $S_{AB}(q)$ as a function of $\varepsilon_{AB}/(k_BT)$, showing increasingly sharp sinusoid-like behavior with $\varepsilon_{AB}/(k_BT)$, corresponding to increasing phase segregation in A–C. (E) $S_{AB}[q; \varepsilon_{AB}/(k_BT)] - S_{AB}(q; 0.5)$ (lines) and Lorentzian fits (dashed, dotted curves), along with domain spacing. Domain spacing increases with increasing incompatibility, consistent with more clearly separated phases in C.

by the arithmetic mixing rule using each particle's native LJ radius: $\sigma_{ij} = 0.5\ (\sigma_i + \sigma_j)$. To crudely simulate the size disparities found in a PEO–lithium bistriflimide system, we chose $\sigma_A = \sigma_B = \sigma$, $\sigma_c = 0.5\ \sigma$, and $\sigma_a = 1.5\ \sigma$. All LJ energies $\varepsilon_{ij} = 1.0\ k_BT$, except ε_{AB}. Inspired by work of Grest et al. and others,[34,36−38] we chose $\varepsilon_{AB} = [0.5, 1.0, 1.5]\ k_BT$ to vary the incompatibility between monomers A and B. Namely, a low value of ε_{AB} promotes compatibility, while a higher value increased incompatibility.

The form of $E_{el}(r_{ij})$ varied with the types of particles i and j. If both particles were ions, they interacted through Coulomb's law

$$E_{el}(r_{ij}) = \frac{q_i q_j}{4\pi\epsilon_0 r_{ij}^2} \tag{5}$$

If one particle i is a monomer and particle j is an ion, they interact through the following potential

$$E_{el}(r_{ij}) = \frac{q_j(\boldsymbol{\mu}_i \cdot \mathbf{r}_{ij})}{4\pi\epsilon_0 r_{ij}^3} \tag{6}$$

where $\boldsymbol{\mu}_i$ is the dipole moment vector and $\mathbf{r}_{ij}$ is the displacement vector between particles i and j. A torque on particle i, $\mathbf{T}_{ij}$, was also induced by this potential

$$\mathbf{T}_{ij} = \frac{q_j(\boldsymbol{\mu}_i \times \mathbf{r}_{ij})}{4\pi\epsilon_0 r_{ij}^3} \tag{7}$$

Finally, if both particles were monomers, they interacted through the following potential

$$E_{el}(r_{ij}) = \frac{1}{4\pi\epsilon_0 r_{ij}^3}\left[(\boldsymbol{\mu}_i \cdot \boldsymbol{\mu}_j) - \frac{3}{r_{ij}^3}(\boldsymbol{\mu}_i \cdot \mathbf{r}_{ij})(\boldsymbol{\mu}_j \cdot \mathbf{r}_{ij})\right] \tag{8}$$

Similarly, a torque is generated for both particles i and j. The torque on i is calculated according to the following equation

$$\mathbf{T}_{ij} = \frac{1}{4\pi\epsilon_0 r_{ij}^3}\left[-(\boldsymbol{\mu}_i \times \boldsymbol{\mu}_j) + \frac{3}{r_{ij}^3}(\boldsymbol{\mu}_i \times \mathbf{r}_{ij})(\boldsymbol{\mu}_j \cdot \mathbf{r}_{ij})\right] \tag{9}$$

Exchange i with j in the above equation to gain the torque on j $\mathbf{T}_{ji}$. We chose the moment of inertia $I = 0.025\ m\sigma^2$ to propagate torques into rotational motion in each monomer unit.[31] All electrostatics were calculated directly within a 6 σ range. Long-range electrostatics beyond this cutoff was calculated using Ewald summation.[39,40]

Finally, all-bonded particles interacted through the finitely extensible nonlinear elastic bonded spring potential

$$E_{FENE}(r_{ij}) = \frac{1}{2}kR_0^2 \ln\left[1 - \left(\frac{r_{ij}}{R_0}\right)^2\right], \qquad r_{ij} \le R_0 \tag{10}$$

The spring constant k and the maximum extension R_0 were chosen to be 30 ε/σ^2 and 1.5 σ, respectively.[41]

We simulated all systems in the Large-scale Atomic/Molecular Massively Parallel Simulator package.[42] All simu-

https://dx.doi.org/10.1021/acs.macromol.9b02510
Macromolecules 2020, 53, 875−884

Table 1. Summary of the Miscibilities of All Simulated Blend Electrolytes as Functions of Polarity Contrast $\Delta\mu/\mu_{EO}$, Relative Composition Φ_A, and Incompatibility $\varepsilon_{AB}/(k_BT)$[a]

$\Delta\mu/\mu_{EO}$		0.1			0.4			0.8		
ε_{AB}/k_BT		0.5	1.0	1.5	0.5	1.0	1.5	0.5	1.0	1.5
Φ_A (%)	25	M	M	I	M	M	I	M	I	I
	50	M	M	I	M	I	I	M	I	I
	75	M	I	I	M	I	I	M	I	I

[a]Miscible and Immiscible Blends are Denoted by Black M's and Red I's, Respectively

lations consisted of N = 100 chains with 20 RUs and 125 ion pairs, yielding [RU]/[c] = 16. The number of chains of type A N_A was determined by the relative volume percentage Φ_A = 100 (N_A/N)% = [0, 25, 50, 75, 100] %. Each simulation box was initially packed with random polymer configurations, after which ions were randomly dispersed, resulting in a total number density of ρ = 0.85 σ^{-3}. To remove any strong overlaps between neighbors, we minimized each system using the steepest descent algorithm followed by the conjugate gradient algorithm, both with a relative error of 1×10^{-5}. All particles were randomly imparted with a velocity corresponding to a Gaussian distribution yielding T^* = 1.0 k_BT/ε for both linear and rotational degrees of freedom. Each system was equilibrated for 1.5×10^5 τ with a timestep 0.01 τ in an *NVT* ensemble using the Nosé–Hoover thermostat on both linear and rotational degrees of freedom.[43,44] Each system was run an additional 5×10^5 τ to produce trajectories for further analysis. We reported the positions of each particle every 5 τ. We ran each system at a given value of Φ_A, $\Delta\mu/\mu_{EO}$, and $\varepsilon_{AB}/(k_BT)$ in triplicate with unique starting configurations and assignments of linear and angular velocities.

RESULTS AND DISCUSSION

Determining Blend Miscibility. We first examined the miscibility of the polymer blend electrolytes. At first, we sought to qualitatively infer miscibility by visually examining snapshots of the blend electrolyte simulations. We can see in Figure 1A–C, which shows snapshots of blends with a modest polarity contrast of $\Delta\mu/\mu_{EO}$ = 0.4, that low- and high-polarity polymers seem to increasingly phase segregate with increasing $\varepsilon_{AB}/(k_BT)$, which aligns with intuition derived from Grest et al.[34]

We next sought to more quantitatively describe phase segregation in each of these simulations by employing some measures that quantifies the correlations between each monomer type. Usage of a linear density profile has found good success in the previous simulation literature to locate the boundaries between different phases in lamellae-forming block copolymers.[45−48] However, as can be seen in Figure 1B, the two phases do not necessarily align themselves perpendicular to a given direction in the simulation box, a necessary precondition for such an analysis. A more appropriate measure is the partial structure factor $S_{AB}(q)$ and the Fourier transform of the radial distribution function between monomer beads of types A and B $g_{AB}(r)$

$$S_{AB}(q) = 8\pi\rho x_A x_B \int_0^\infty \frac{\sin qr}{qr} r^2 w(r)[g_{AB}(r) - 1]\mathrm{d}r \quad (11)$$

where x_i is the mole fraction of species type i and ρ is the total system number density (0.85 σ^{-3}). The revised Lorch window $w(r)$ was used to eliminate the cutoff ripple artifact due to $g_{AB}(r)$ not approaching unity at large r and was defined as

$$w(r) = \frac{3}{(2\pi r/L)^3}\left[\sin\left(\frac{2\pi r}{L}\right) - \left(\frac{2\pi r}{L}\right)\cos\left(\frac{2\pi r}{L}\right)\right] \quad (12)$$

where L is the box length of each simulation.[49] As the maximum distance r in $g_{AB}(r)$ is limited to $L/2$, we set the minimum $q_{min} = 2\pi/(L/2)$ σ^{-1}. The maximum q was chosen to correspond to LJ radius of the cation: $q_{max} = 2\pi/(0.5)$ σ^{-1}.

We plot the results of such a calculation in Figure 1D for $\Delta\mu/\mu_{EO}$ = 0.4. The remaining profiles can be found in Figure S1. At low incompatibility, this function is smooth with one clear structural feature located at ~7 σ^{-1} ($d \approx 2\pi/7 = 0.9$ σ), which roughly corresponds to monomer–monomer contact. As incompatibility increases, the $S_{AB}(q)$ profile gains a sinusoid-like contribution, seen most strongly in the scattering pattern for $\varepsilon_{AB}/(k_BT)$ = 1.5, which grows stronger with increasing visually determined phase segregation, as seen in Figure 1A–C. Given this strong correlation, we intended to use such a pattern as a proxy to determine if each simulation is phase-separated.

We noted, however, that this sinusoid-like pattern is sometimes fairly weak, as observed for the $\varepsilon_{AB}/(k_BT)$ = 1.0 case and others in Figure S1, and is overshadowed by the majority of the scattering arising from monomer–monomer correlations. We proposed then to crudely "normalize" the scattering of higher incompatibility blends by subtracting from them the scattering profile of their corresponding $\varepsilon_{AB}/(k_BT)$ = 0.5 case, thus keeping only scattering arising from phase separation, if it exists at all. We expected that phase-segregated systems would maintain their sinusoid-like pattern after subtraction, whereas those that are not phase-segregated would not contain such scattering. An example of such a "normalization" is shown in Figure 1E, wherein clear repeating peaks emerge for both electrolytes after subtraction by $S_{AB}(q; \varepsilon_{AB}/(k_BT) = 0.5)$. We fit the first peak to a Lorentzian to extract the domain sizing. The domain sizing increases with increasing incompatibility, as we would anticipate larger volumes of low- and high-polarity polymer-rich phases. We present normalized $S_{AB}(q)$ profiles for the remaining blends in Figure S2 and summarize the miscibilities of all blends in Table 1 above. In short, the overall trends from these results suggest two main results: (A) immiscibility tends to increase with increasing relative content Φ_A and (B) lower polarity contrast encourages mixing.

Determining an Ion's Local Environment. As noted in the Introduction, the local environment around an ion is a likely determinant in the synergy between high-mobility and high-polarity components in blend SMEs, wherein the high-polarity component solvates the cation and the high-mobility

https://dx.doi.org/10.1021/acs.macromol.9b02510
Macromolecules 2020, 53, 875−884

component provides a low viscosity environment through which the cation can quickly diffuse.

Toward a validation of the abovementioned hypothesis, we quantified the local ion environment by using a distance-based cluster analysis. We calculated a local connectivity matrix m, which tagged all monomer beads of type A and B within some distance cutoff of a cation. We chose two cutoffs, 1.80 σ and 2.75 σ, representative as the extent of the first and second solvation shells. These shells were chosen as the approximate cutoffs of the first and second minima of the cation−monomer $g(r)$, respectively, which are shown in Figure S3 for Φ_A = 50%. From m, we count the number of both monomer bead types ($\hat{N}_A$, $\hat{N}_B$) to calculate the local relative volume fraction of A: $\hat{\phi}_A = \hat{N}_A/(\hat{N}_A + \hat{N}_B)$. From these data, we count all of the instances of $\hat{\phi}_A$ ($N(\hat{\phi}_A)$) to generate a probability distribution of a given local volume fraction of A $p(\hat{\phi}_A)$

$$p(\hat{\phi}_A) = \frac{N(\hat{\phi}_A)}{\sum_{\hat{\phi}_A} N(\hat{\phi}_A)} \tag{13}$$

In the cases in which there is no monomer bead within the desired cutoff, they were counted separately and were assigned a probability $p(\varnothing)$ as described above. In all cases $p(\varnothing) < 10^{-4}$. As a summary of these distributions, we also calculated the average local volume fraction of A

$$\bar{\phi}_A = \frac{\sum_{\hat{\phi}_A} p(\hat{\phi}_A)\hat{\phi}_A}{\sum_{\hat{\phi}_A} p(\hat{\phi}_A)} \tag{14}$$

We plot $\bar{\phi}_A$ as a function of $\Delta\mu/\mu_{EO}$ and $\varepsilon_{AB}/(k_BT)$ in Figure 2A−B for Φ_A = 50%. Results for Φ_A = 25% and Φ_A = 75% can be seen in Figure S4. For the shorter cutoff, as shown in Figure 2A, we can see that first solvation shell around cations consist predominantly of high-polarity polymer B (note that all $\bar{\phi}_A$ < 0.5). Such results and previous findings in SMEs[3,5,47] and dilute PBEs[29] are consistent with our proposition that the high-polarity polymer would be the favored coordinating species relative to the high-mobility polymer. As evidenced by the value of $\bar{\phi}_A$ with increasing incompatibility at a fixed $\Delta\mu/\mu_{EO}$, these results further suggest that increasing the incompatibility of the polymer blend causes ions to more strongly interact with the high-polarity polymer. We note that, given the total immiscibility at high incompatibility, these results more strongly imply that ions are partitioning into a high-polarity, ion-rich phase, consistent with previous findings.[4,47] When we examine the total content of both the first and second solvation shells, as seen in Figure 2B, we can see that there is an enrichment of the high-mobility polymer A. As anticipated, it seems that cations are surrounded by a sheath of the PBE host enriched in polymer A outside its first solvation shell.

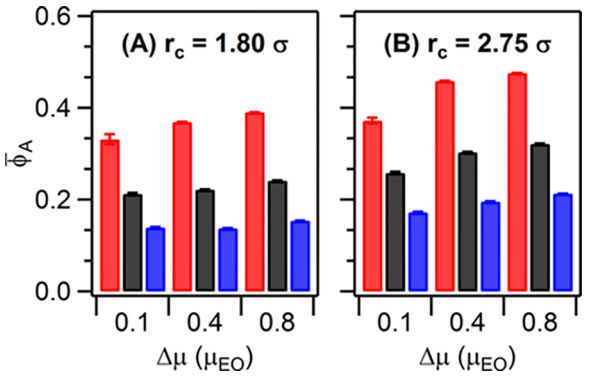

Figure 2. Average relative environment $\bar{\phi}_A$ as a function of polarity contrast and polymer host incompatibilities $\varepsilon_{AB}/(k_BT)$ using a cutoff of (A) 1.80 σ and (B) 2.75 σ. Red, black, and blue bars represent $\varepsilon_{AB}/(k_BT)$ values of 0.5, 1.0, and 1.5, respectively.

Ionic Transport in Polymer Blends. Given the abovementioned findings, we sought to quantify ionic transport and identify its correlations with miscibility and the local ion environment. To quantify ionic transport, we calculated the ionic conductivity $\lambda = \alpha\lambda_{NE}$, where α is the degree of the uncorrelated motion (see eq 15) and λ_{NE} is the Nernst−Einstein conductivity (see eq 16). α is defined as the ratio of the charge-scaled cross-correlated and self-correlated mean-squared displacements

$$\alpha = \lim_{t\to\infty} \frac{\sum_{i,j} q_i q_j \langle [\mathbf{r}_i(t) - \mathbf{r}_i(0)]\cdot[\mathbf{r}_j(t) - \mathbf{r}_j(0)]\rangle}{\sum_i q_i^2 \langle \|\mathbf{r}_i(t) - \mathbf{r}_i(0)\|^2 \rangle} \tag{15}$$

As has been discussed in the previous literature, accurate calculation of α is challenging because of the poor long-time statistics of the numerator of eq 15. Instead, we calculate both the numerator and denominator using short-time statistics, corresponding to $t \leq 0.05t_{sim}$, where t_{sim} is the total simulation time, and we take their ratio to estimate α.[9,10,50−54] We calculated λ_{NE} according to the following expression

$$\lambda_{NE} = \frac{e^2}{Vk_BT}(N_cD_c + N_aD_a) \tag{16}$$

where V is the system volume and N_i is the number of ions of type i. The diffusion coefficients D_i are calculated by taking the long-time slope of self-correlated mean-squared displacement

$$D_i = \lim_{t\to\infty} \frac{1}{6N_i}\frac{d}{dt}\sum_{j=1}^{N_i} \langle \left\|\mathbf{r}_{ij}(t) - \mathbf{r}_{ij}(0)\right\|^2 \rangle \tag{17}$$

We plot the results for α and D_i in Figures S5 and S6, respectively, in the Supporting Information.

We display the conductivity λ in Figure 3 as a function of relative composition Φ_A for $\Delta\mu/\mu_{EO}$ of (A) 0.1, (B) 0.4, and (C) 0.8. We recall our observation that miscible-blend PBEs had an ion environment most enriched in the high-polarity polymer within the first solvation shell. Based on the hypothesis discussed in the introduction, we would expect that these blend PBEs would have the highest ionic conductivities relative to more incompatible blend PBEs. We would further expect that these improved conductivities may be greater than those of their corresponding pure PBEs. Our expectations are indeed seen to be validated in the case of middle- (Figure 3B) and high- (Figure 3C) polarity contrasts. This effect is strong enough in the highest polarity contrast systems that the ionic conductivity seems to positively deviate relative to the linear mixing rule, signified by the black dashed line.

In contrast to the above findings, we note that in the lowest polarity contrast blend, λ (Figure 3A) slightly worsens with increasing miscibility (decreasing incompatibility). Given our previous observations on the influence of incompatibility with these blend PBEs' miscibilities and local ion environments (Figure 2), we would have expected similar behavior to the highest polarity contrast blends. The deviation of our results

https://dx.doi.org/10.1021/acs.macromol.9b02510
Macromolecules 2020, 53, 875−884

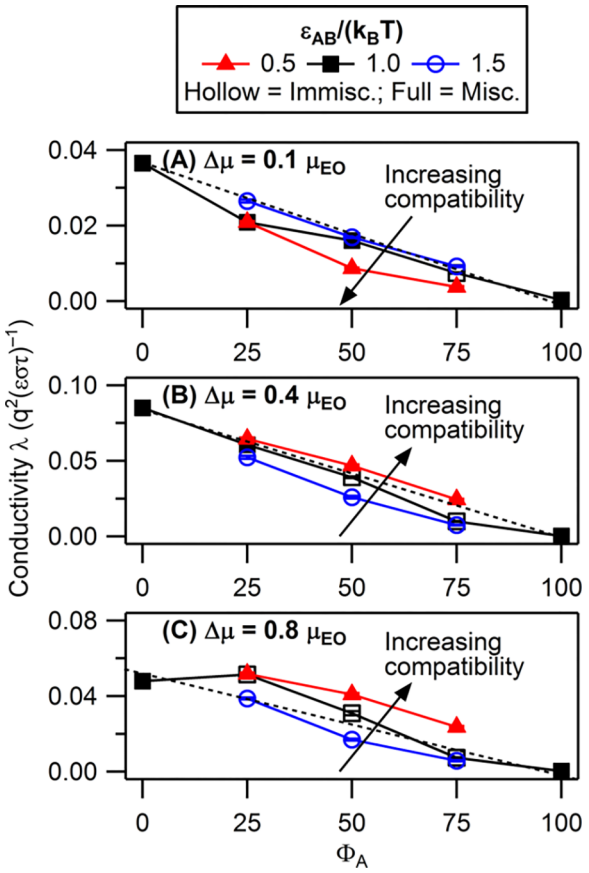

Figure 3. Ionic conductivity λ as a function of relative volume percentage of A Φ_A. Panels represent blend electrolytes at fixed polarity contrasts $\Delta\mu/\mu_{EO}$ of (A) 0.1, (B) 0.4, and (C) 0.8. Red triangles, black squares, and blue circles represent incompatibility strengths $\epsilon_{AB}/(k_BT)$ of 0.5, 1.0, and 1.5, respectively. Error bars shown are standard deviations and are mostly hidden by their respective symbols. Filled and hollow symbols represent miscible and immiscible systems, respectively. Dashed lines represent the linear mixing rule between the pure blend electrolytes. Increasing compatibility slightly worsens ionic conductivity in low-polarity contrast electrolytes, as seen in A, but improves ionic conductivity in higher contrast polarity electrolytes, as seen in B and C.

from such expectations suggests that there must be some factors in these blends that differs from the highest polarity contrast blends. In the subsequent sections, we examine the roles of polymer dynamics and ion aggregation to understand the deviations noted in low-polarity contrast blends.

Role of Polymer Dynamics and Ionic Aggregation in the Observed Trends in Ionic Transport. We first begin by examining polymer dynamics in the simulated PBEs. We calculated polymer dynamics for each polymer type in our blend electrolyte simulations by first calculating the self-part of the dynamic structure factor $S_i(q = 2\pi/5.0\ \sigma^{-1}, t)$

$$S_i(q, t) = \frac{1}{N_i}\left\langle \sum_{j=1}^{N_i} \frac{\sin(q\|\mathbf{r}_{ij}(t) - \mathbf{r}_{ij}(0)\|)}{q\|\mathbf{r}_{ij}(t) - \mathbf{r}_{ij}(0)\|} \right\rangle \quad (18)$$

where i is either a monomer bead of type A or B and N_i is the number of polymer beads of type i. We fit $S_i(q, t) \geq 0.05$ to a stretched exponential[55,56]

$$S_i(q, t) = \exp\left[-\left(\frac{t}{ti^*}\right)^{\beta_i}\right] \quad (19)$$

where t_i^* is a characteristic timescale and β_i is the stretching exponent. We extracted a relaxation rate $\tau_{R,i}^{-1}$ according to the following equation

$$\tau_{R,i}^{-1} = \left[\frac{t_i^*}{\beta_i}\Gamma\left(\frac{1}{\beta_i}\right)\right]^{-1} \quad (20)$$

where $\Gamma(x)$ is the gamma function with argument x.

We present the results of the above calculations in Figure 4 as a function of relative composition Φ_A. We first observe that the dynamics of the low-polarity polymers (signified by the curves with solid lines) are rather insensitive to relative blend composition, polarity contrast, and host incompatibilities. These results are broadly consistent with our hypothesis and

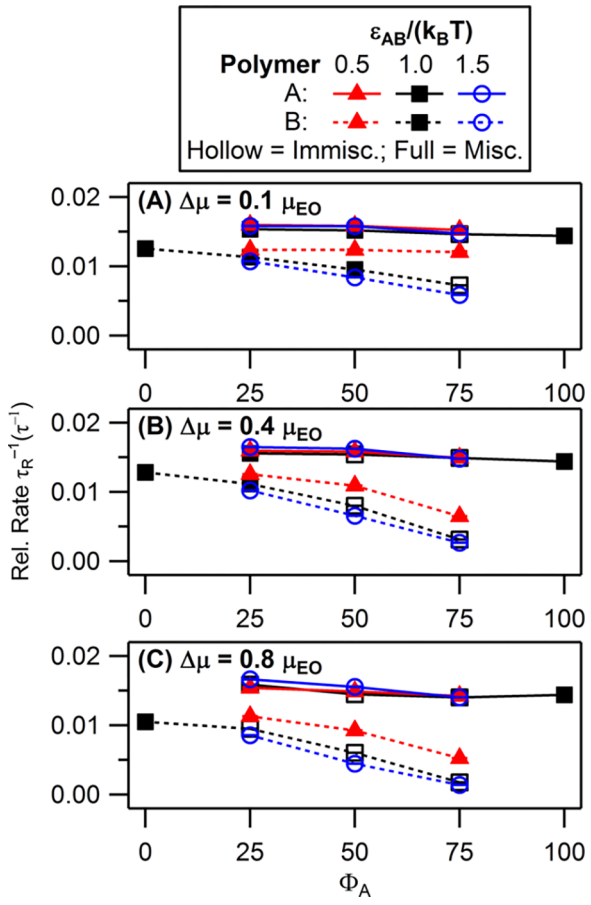

Figure 4. Polymer relaxation rates τ_R^{-1} as a function of relative volume percentage of A Φ_A. Panels represent blend electrolytes at fixed polarity contrasts $\Delta\mu/\mu_{EO}$ of (A) 0.1, (B) 0.4, and (C) 0.8. Red triangles, black squares, and blue circles represent incompatibility strengths $\epsilon_{AB}/(k_BT)$ of 0.5, 1.0, and 1.5, respectively. Error bars shown are standard deviations and are mostly hidden by their respective symbols. Filled and hollow symbols represent miscible and immiscible systems, respectively. Solid and dashed curves represent low- and high-polarity polymers, respectively. Increasing compatibility similarly improves high-polarity polymer dynamics in all electrolytes and has little influence on the dynamics of the low-polarity polymer, suggesting that the observed changes in ionic conductivity are less likely to originate from changes in polymer dynamics.

https://dx.doi.org/10.1021/acs.macromol.9b02510
Macromolecules 2020, 53, 875−884

previous findings:[9] the exclusion of ions from the low-polarity polymer keeps their dynamics unchanged. Second, we observe that dynamics of the high-polarity polymer improves with decreasing $\varepsilon_{AB}/(k_BT)$ at a given Φ_A and $\Delta\mu/\mu_{EO}$. We hypothesized that the dynamics near the ion (i.e., the high-polarity polymer) should improve because of the presence of the high-mobility polymer in miscible blend PBEs; overall, this final result suggests that this is indeed the case.

More pertinently, the abovementioned results indicate that regardless of the contrast between the polymer hosts, the addition of the low-polarity, high-mobility polymer should improve the polymer mobilities and hence the ionic conductivity of the most compatible PBEs. However, the observed trends, seen in Figure 3, contrast with such expectations and show that the benefits of high-polarity plasticization in low-polarity contrast blends is offset by some other factors. In an effort to rationalize our ionic conductivity results, we turn to the ionic aggregation properties of these blend electrolytes.

As a measure of ionic aggregation in our system, we calculated the average ionic cluster size $\bar{n}$. To determine this measure, we used a similar distance-based cluster analysis to the local-ion environment analysis. We again generated a local connectivity matrix m that tracks cation−anion pairs over the course of our simulations. A pair is defined as a cation and anion whose distance is less than 1.25 σ, a cutoff chosen based the minimum of the radial distribution function between these species calculated in previous work.[10,28] We then generated a global connectivity matrix M using an algorithm initially developed by Sevick et al.,[9,10,28,57−59] which defines aggregates of ions connected through the topology defined by the m. From M, we determined $N(n)$, which is the number of aggregates of size n (n = 1 is a free ion). We calculated the average ionic size $\bar{n}$ according to the following equation

$$\bar{n} = \frac{\sum_n^{N_a+N_c} N^2(n)n}{\sum_n^{N_a+N_c} N(n)n} \tag{21}$$

The results of the above calculation are displayed in Figure 5 as a function of relative composition Φ_A. From these results, we can see that ionic aggregation remains essentially the same or is slightly improved with decreased incompatibility between hosts in middle- (Figure 5B) and high- (Figure 5C) polarity contrast electrolytes. Consistent with our hypothesis, we also note that ionic aggregation is much more characteristic of the high-polarity host B at most compositions in both miscible and immiscible blends. We thus conclude that consistently low ionic aggregation in higher polarity contrast blends thus couples ionic transport to the dynamics presented in Figure 4, leading to the improved ionic conductivity observed in Figure 3.

However, the abovementioned observations change in the case of lowest polarity contrast blend PBEs (Figure 5A). In particular, ionic aggregation worsens with decreasing incompatibility at all compositions. We additionally observe that ionic aggregation at intermediate compositions seems to be a mixture of aggregation from both pure electrolytes, in contrast to the higher polarity contrast electrolytes. We note that the lowest polarity contrast blend was chosen so that the high-polarity polymer B only slightly better solvates ions in comparison to its blend partner. Improving miscibility brings polymer A into more contact with ions. Because of the already weak interactions between B and ions as well as the increased

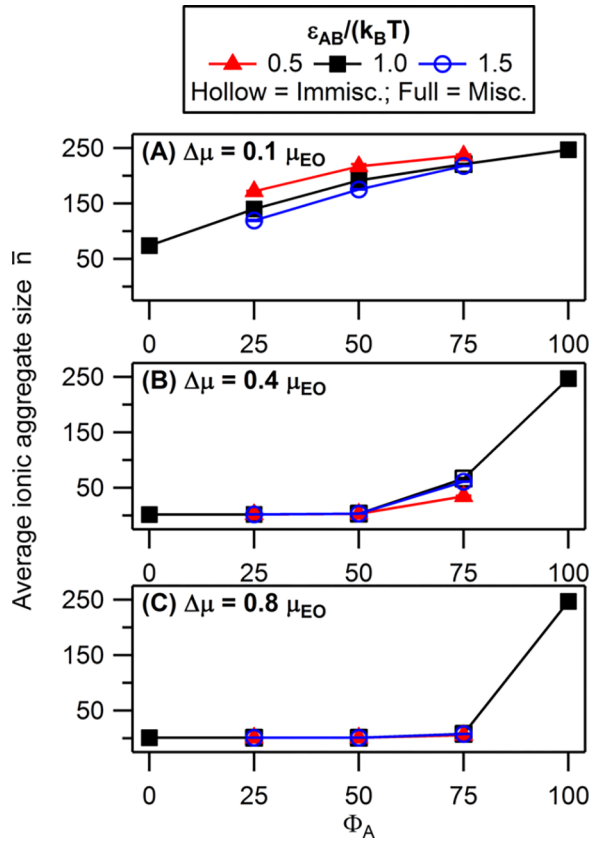

Figure 5. Average ionic aggregate size $\bar{n}$ as a function of relative volume percentage of Φ_A. Panels represent blend electrolytes at fixed polarity contrasts $\Delta\mu/\mu_{EO}$ of (A) 0.1, (B) 0.4, and (C) 0.8. Red triangles, black squares, and blue circles represent incompatibility strengths $\varepsilon_{AB}/(k_BT)$ of 0.5, 1.0, and 1.5, respectively. Error bars shown are standard deviations and are mostly hidden by their respective symbols. Increasing compatibility worsens ionic aggregation in low-polarity contrast electrolytes, as seen in A, while having a little effect in higher contrast electrolytes, as seen in B and C. This suggests that worsened ionic conductivity, as shown in Figure 3A, arises from extensive ionic aggregation.

concentration of A near ions, aggregation worsens with decreasing $\varepsilon_{AB}/(k_BT)$ at fixed Φ_A. Overall, these results suggest that the observation in Figure 3 that ionic conductivity slightly worsens in the lowest polarity contrast systems is due to the extensive ionic aggregation present in low-polarity contrast electrolytes.

Finally, because $\lambda \propto \alpha\sum_i D_i$, aggregation can influence λ through either α or D_i. From the results displayed in Figure S6, D_i follows the trends seen for λ in Figure 3. Such an observation, in conjunction with the abovementioned discussion, suggests that ionic aggregation directly impacts the ion mobilities and thereby the ionic conductivities. Surprisingly, we observe that α (Figure S5) actually increases with $\varepsilon_{AB}/(k_BT)$ for all $\Delta\mu/\mu_{EO}$, which contrasts with the results of our previous work which has noted α and ionic aggregation to be inversely correlated with each other.[9,10,28] To rationalize the results of our present study, we note that because ionic aggregation is a static measure while α is a dynamic property, there is no a priori reason why they must be correlated with each other in all cases. As an example, Fong and co-workers saw that static and dynamic measures of ionic aggregation did not necessarily correlate with each other.[60] Inspired by their work, we calculated the cationic diffusion length, defined as

https://dx.doi.org/10.1021/acs.macromol.9b02510
Macromolecules 2020, 53, 875−884

$L_c = \sqrt{6D_c\tau_C}$, where τ_C is the ion-pair association time (see eqs S1−S3). Such a dynamic measure can be interpreted as the length scale over which a cation typically diffuses while remaining associated with a counteranion. We expected cations to remain associated with anions over shorter length scales in electrolytes with less-correlated ionic motion. Indeed, as can be seen in Figure S7, L_c seems to be roughly inversely correlated with α. These low-polarity electrolytes in which static ionic aggregation worsens while α improves maintain a relatively low dynamic correlated motion L_c (red triangles), which may explain such a trend.

CONCLUSIONS

In summary, inspired by the success of small-molecule battery electrolytes, we hypothesized that polymer electrolytes consisting of a miscible blend of a high-mobility component and a high-polarity component would experience improvements in ionic transport in comparison to their immiscible counterparts. We proposed that this would arise due to a synergy between the two hosts. First, the high-polarity polymer would strongly coordinate ions, leading to low ionic aggregation consistent with pure electrolytes consisting of only high-polarity polymer. Second, the high-mobility component, excluded from this interaction, would improve electrolyte dynamics. Together, these two effects would improve ion transport.

To validate the above hypothesis, we simulated a set of coarse-grained, ternary polymer-polymer-salt blend electrolytes. We found that, in sufficiently high-polarity contrast electrolytes, our expectations were confirmed: ionic conductivity increases with decreasing incompatibility (increasing miscibility). The local environment around cations was enriched in the high-polarity polymer even in miscible blends, which yielded ionic aggregation consistent with an electrolyte containing only the high-polarity polymer. The excluded high-mobility component improved the dynamics of the electrolyte, thereby improving ionic mobility.

In contrast to the above results for high-polarity contrast blends, the results for the lowest polarity contrast electrolytes did not accord with our hypothesis. Although we observed improvements in electrolyte dynamics similar to their higher polarity contrast counterparts, ionic aggregation worsened in low-contrast electrolytes with decreasing incompatibility. We rationalized such results by suggesting that improving miscibility brings polymer A into more contact with ions. Because of the already weak interactions between B and ions as well as the increased concentration of A near ions, aggregation worsens with decreasing $\epsilon_{AB}/(k_BT)$ at fixed Φ_A. Such behavior slowed ionic diffusion, yielding the observed trend in ionic conductivity.

Our work suggests that improvements in polymer electrolytes can be made by blending two hosts. To achieve an enhanced conductivity, the requirements are twofold: first, there must be sufficiently high polarity contrast between the two hosts; second, the polymers must remain miscible with each other. The first requirement is relatively easy to meet: many polyethers have low dielectric constants and low glass-transition temperatures.[8,18] Modifications of these materials to improve polarity can likely be achieved through the addition of functional groups, such as carbonyl, sulfonyl, or cyano groups.[61] As shown by Kumar and others, increasing polarity contrast between the hosts is likely to decrease PBE miscibility.[32,33,62] Thus, to meet the second requirement, strategies to improve miscibility, such as adding hydrogen bonding moieties along the polymer backbone[22] or using salt to compatibilize particularly high-contrast blends,[23] should be employed.

ASSOCIATED CONTENT

Supporting Information

The Supporting Information is available free of charge at https://pubs.acs.org/doi/10.1021/acs.macromol.9b02510.

Additional PBE structure factor and ion environment data, monomer−cation radial distribution functions, degrees of uncorrelated motion, ionic diffusion coefficients, and diffusion lengths (PDF)

AUTHOR INFORMATION

Corresponding Author

Venkat Ganesan − *The University of Texas at Austin, Austin, Texas;* orcid.org/0000-0003-3899-5843; Email: venkat@che.utexas.edu

Other Authors

Bill K. Wheatle − *The University of Texas at Austin, Austin, Texas;* orcid.org/0000-0003-0550-4905

Nathaniel A. Lynd − *The University of Texas at Austin, Austin, Texas;* orcid.org/0000-0003-3010-5068

Complete contact information is available at: https://pubs.acs.org/10.1021/acs.macromol.9b02510

Notes

The authors declare no competing financial interest.

ACKNOWLEDGMENTS

The National Science Foundation (grants DMR-1721512 and CBET-17069698) and the Robert A. Welch Foundation (grants F-1599 and F-1904) both supported this work. The results in this paper were generated using high-performance computing resources provided by The University of Texas at Austin Texas Advanced Computing Center.

REFERENCES

(1) Goodenough, J. B.; Kim, Y. Challenges for Rechargeable Li Batteries. *Chem. Mater.* **2010**, *22*, 587−603.

(2) Xu, K. Nonaqueous liquid electrolytes for lithium-based rechargeable batteries. *Chem. Rev.* **2004**, *104*, 4303−4418.

(3) Xu, K. Electrolytes and Interphases in Li-Ion Batteries and Beyond. *Chem. Rev.* **2014**, *114*, 11503−11618.

(4) Nakamura, I.; Balsara, N. P.; Wang, Z.-g. Thermodynamics of Ion-Containing Polymer Blends and Block Copolymers. *Phys. Rev. Lett.* **2011**, *107*, 198301.

(5) Franco, A. A.; Rucci, A.; Brandell, D.; Frayret, C.; Gaberscek, M.; Jankowski, P.; Johansson, P. Boosting Rechargeable Batteries R&D by Multiscale Modeling: Myth or Reality? *Chem. Rev.* **2019**, *119*, 4569−4627.

(6) Sax, J.; Ottino, J. M. Modeling of transport of small molecules in polymer blends: Application of effective medium theory. *Polym. Eng. Sci.* **1983**, *23*, 165−176.

(7) Hallinan, D. T.; Balsara, N. P. Polymer Electrolytes. *Annu. Rev. Mater. Res.* **2013**, *43*, 503−525.

(8) Barteau, K. P. Poly(Glycidyl Ether)-Based Battery Electrolytes: Correlating Polymer Properties to Ion Transport. Ph.D. thesis, University of California, Santa Barbara, 2015.

(9) Wheatle, B. K.; Keith, J. R.; Mogurampelly, S.; Lynd, N. A.; Ganesan, V. Influence of Dielectric Constant on Ionic Transport in Polyether-Based Electrolytes. *ACS Macro Lett.* **2017**, *6*, 1362−1367.
(10) Wheatle, B. K.; Lynd, N. A.; Ganesan, V. Effect of Polymer Polarity on Ion Transport: A Competition between Ion Aggregation and Polymer Segmental Dynamics. *ACS Macro Lett.* **2018**, *7*, 1149−1154.
(11) Aziz, S. B.; Woo, T. J.; Kadir, M. F. Z.; Ahmed, H. M. A conceptual review on polymer electrolytes and ion transport models. *J. Sci. Adv. Mater. Devices* **2018**, *3*, 1−17.
(12) Zhang, H.; Chen, F.; Lakuntza, O.; Oteo, U.; Qiao, L.; Martinez-Ibañez, M.; Zhu, H.; Carrasco, J.; Forsyth, M.; Armand, M. Suppressed Mobility of Negative Charges in Polymer Electrolytes with an Ether-Functionalized Anion. *Angew. Chem., Int. Ed.* **2019**, *58*, 11926.
(13) Bhandary, R.; Schönhoff, M. Polymer effect on lithium ion dynamics in gel polymer electrolytes: Cationic versus acrylate polymer. *Electrochim. Acta* **2015**, *174*, 753−761.
(14) Sun, J.; Stone, G. M.; Balsara, N. P.; Zuckermann, R. N. Structure-Conductivity Relationship for Peptoid-Based PEO-Mimetic Polymer Electrolytes. *Macromolecules* **2012**, *45*, 5151−5156.
(15) Teran, A. A.; Tang, M. H.; Mullin, S. A.; Balsara, N. P. Effect of Molecular Weight on Conductivity of Polymer Electrolytes. *Solid State Ionics* **2011**, *203*, 18−21.
(16) Timachova, K.; Watanabe, H.; Balsara, N. P. Effect of Molecular Weight and Salt Concentration on Ion Transport and the Transference Number in Polymer Electrolytes. *Macromolecules* **2015**, *48*, 7882−7888.
(17) O'Reilly, M. V.; Masser, H.; King, D. R.; Painter, P. C.; Colby, R. H.; Winey, K. I.; Runt, J. Ionic Aggregate Dissolution and Conduction in a Plasticized Single-Ion Polymer Conductor. *Polymer* **2015**, *59*, 133−143.
(18) Barteau, K. P.; Wolffs, M.; Lynd, N. A.; Fredrickson, G. H.; Kramer, E. J.; Hawker, C. J. Allyl Glycidyl Ether-Based Polymer Electrolytes for Room Temperature Lithium Batteries. *Macromolecules* **2013**, *46*, 8988−8994.
(19) Thelen, J. L.; Inceoglu, S.; Venkatesan, N. R.; Mackay, N. G.; Balsara, N. P. Relationship between Ion Dissociation, Melt Morphology, and Electrochemical Performance of Lithium and Magnesium Single-Ion Conducting Block Copolymers. *Macromolecules* **2016**, *49*, 9139−9147.
(20) Sarapas, J. M.; Tew, G. N. Poly(ether-thioethers) by Thiol-Ene Click and Their Oxidized Analogues as Lithium Polymer Electrolytes. *Macromolecules* **2016**, *49*, 1154−1162.
(21) Flory, P. J. Themodynamics of high polymer solutions. *J. Chem. Phys.* **1942**, *10*, 51−61.
(22) He, Y.; Zhu, B.; Inoue, Y. Hydrogen bonds in polymer blends. *Prog. Polym. Sci.* **2004**, *29*, 1021−1051.
(23) Wang, Z.-G. Effects of ion solvation on the miscibility of binary polymer blends. *J. Phys. Chem. B* **2008**, *112*, 16205−16213.
(24) Stockmayer, W. H. Second virial coefficients of polar gases. *J. Chem. Phys.* **1941**, *9*, 398−402.
(25) Stockmayer, W. H. Dielectric Dispersion in Solutions of Flexible Polymers. *Pure Appl. Chem.* **1967**, *15*, 539−554.
(26) Gordievskaya, Y. D.; Budkov, Y. A.; Kramarenko, E. Y. An interplay of electrostatic and excluded volume interactions in the conformational behavior of a dipolar chain: Theory and computer simulations. *Soft Matter* **2018**, *14*, 3232−3235.
(27) Budkov, Y. A.; Kiselev, M. G. Flory-type theories of polymer chains under different external stimuli. *J. Phys. Condens. Matter* **2018**, *30*, 043001.
(28) Wheatle, B. K.; Fuentes, E. F.; Lynd, N. A.; Ganesan, V. Influence of Host Polarity on Correlating Salt Concentration, Molecular Weight, and Molar Conductivity in Polymer Electrolytes. *ACS Macro Lett.* **2019**, *8*, 888−892.
(29) Nakamura, I. Ion solvation in polymer blends and block copolymer melts: Effects of chain length and connectivity on the reorganization of dipoles. *J. Phys. Chem. B* **2014**, *118*, 5787−5796.
(30) Nakamura, I. Synergistic effects of ion pairs on the dielectric properties of diblock copolymer melts. *Soft Matter* **2014**, *10*, 9596−9600.
(31) Liu, L.; Nakamura, I. Solvation Energy of Ions in Polymers: Effects of Chain Length and Connectivity on Saturated Dipoles Near Ions. *J. Phys. Chem. B* **2017**, *121*, 3142.
(32) Kumar, R.; Sumpter, B. G.; Muthukumar, M. Enhanced phase segregation induced by dipolar interactions in polymer blends. *Macromolecules* **2014**, *47*, 6491−6502.
(33) Israelachvili, J. N. *Intermolecular and Surface Forces: Revised*, 3rd ed.; Elsevier Science and Technology, 2011.
(34) Grest, G. S.; Lacasse, M. D.; Kremer, K.; Gupta, A. M. Efficient continuum model for simulating polymer blends and copolymers. *J. Chem. Phys.* **1996**, *105*, 10583−10594.
(35) Weeks, J. D.; Chandler, D.; Andersen, H. C. Role of repulsive forces in determining the equilibrium structure of simple liquids. *J. Chem. Phys.* **1971**, *54*, 5237−5247.
(36) Levine, W. G.; Seo, Y.; Brown, J. R.; Hall, L. M. Effect of sequence dispersity on morphology of tapered diblock copolymers from molecular dynamics simulations. *J. Chem. Phys.* **2016**, *145*, 234907.
(37) Gartner, T. E.; Kubo, T.; Seo, Y.; Tansky, M.; Hall, L. M.; Sumerlin, B. S.; Epps, T. H. Domain Spacing and Composition Profile Behavior in Salt-Doped Cyclic vs Linear Block Polymer Thin Films: A Joint Experimental and Simulation Study. *Macromolecules* **2017**, *50*, 7169−7176.
(38) Ramírez-Hernández, A.; Peters, B. L.; Schneider, L.; Andreev, M.; Schieber, J. D.; Müller, M.; Kröger, M.; De Pablo, J. J. A detailed examination of the topological constraints of lamellae-forming block copolymers. *Macromolecules* **2018**, *51*, 2110−2124.
(39) in't Veld, P. J.; Ismail, A. E.; Grest, G. S. Application of Ewald summations to long-range dispersion forces. *J. Chem. Phys.* **2007**, *127*, 144711.
(40) Toukmaji, A.; Sagui, C.; Board, J.; Darden, T. Efficient particle-mesh Ewald based approach to fixed and induced dipolar interactions. *J. Chem. Phys.* **2000**, *113*, 10913−10927.
(41) Kremer, K.; Grest, G. S. Dynamics of entangled linear polymer melts: A molecular-dynamics simulation. *J. Chem. Phys.* **1990**, *92*, 5057−5086.
(42) Plimpton, S. Fast Parallel Algorithms for Short-Range Molecular-Dynamics. *J. Comput. Phys.* **1995**, *117*, 1−19.
(43) Nosé, S. A Unified Formulation of the Constant Temperature Molecular Dynamics Methods. *J. Chem. Phys.* **1984**, *81*, 511−519.
(44) Hoover, W. G. Canonical Dynamics: Equilibrium Phase-Space Distributions. *Phys. Rev. A: At., Mol., Opt. Phys.* **1985**, *31*, 1695−1697.
(45) Sethuraman, V.; Mogurampelly, S.; Ganesan, V. Multiscale Simulations of Lamellar PS-PEO Block Copolymers Doped with $LiPF_6$ Ions. *Macromolecules* **2017**, *50*, 4542−4554.
(46) Sethuraman, V.; Nguyen, B. H.; Ganesan, V. Coarse-graining in simulations of multicomponent polymer systems. *J. Chem. Phys.* **2014**, *141*, 244904.
(47) Brown, J. R.; Seo, Y.; Hall, L. M. Ion Correlation Effects in Salt-Doped Block Copolymers. *Phys. Rev. Lett.* **2018**, *120*, 127801.
(48) Zhang, Z.; Krajniak, J.; Keith, J. R.; Ganesan, V. Mechanisms of Ion Transport in Block Copolymeric Polymerized Ionic Liquids. *ACS Macro Lett.* **2019**, *8*, 1096−1101.
(49) Soper, A. K.; Barney, E. R. On the use of modification functions when Fourier transforming total scattering data. *J. Appl. Crystallogr.* **2012**, *45*, 1314−1317.
(50) Picálek, J.; Kolafa, J. Molecular Dynamics Study of Conductivity of Ionic Liquids: The Kohlrausch Law. *J. Mol. Liq.* **2007**, *134*, 29−33.
(51) Lesch, V.; Jeremias, S.; Moretti, A.; Passerini, S.; Heuer, A.; Borodin, O. A Combined Theoretical and Experimental Study of the Influence of Different Anion Ratios on Lithium Ion Dynamics in Ionic Liquids. *J. Phys. Chem. B* **2014**, *118*, 7367−7375.
(52) Borodin, O.; Gorecki, W.; Smith, G. D.; Armand, M. Molecular Dynamics Simulation and Pulsed-Field Gradient NMR Studies of Bis(fluorosulfonyl)imide (FSI) and Bis[(trifluoromethyl)sulfonyl]-

https://dx.doi.org/10.1021/acs.macromol.9b02510
Macromolecules 2020, 53, 875−884

imide (TFSI)-Based Ionic Liquids. *J. Phys. Chem. B* **2010**, *114*, 6786−6798.
(53) Li, Z.; Smith, G. D.; Bedrov, D. Li^+ Solvation and Transport Properties in Ionic Liquid/Lithium Salt Mixtures: A Molecular Dynamics Simulation Study. *J. Phys. Chem. B* **2012**, *116*, 12801−12809.
(54) Mogurampelly, S.; Ganesan, V. Effect of Nanoparticles on Ion Transport in Polymer Electrolytes. *Macromolecules* **2015**, *48*, 2773−2786.
(55) Williams, G.; Watts, D. C. Non-Symmetrical Dielectric Relaxation Behaviour Arising from a Simple Empirical Decay Function. *Trans. Faraday Soc.* **1970**, *66*, 80−85.
(56) Williams, G.; Watts, D. C.; Dev, S. B.; North, A. M. Further Considerations of Non Symmetrical Dielectric Relaxation Behaviour Arising from a Simple Empirical Decay Function. *Trans. Faraday Soc.* **1971**, *67*, 1323−1335.
(57) Sevick, E. M.; Monson, P. a.; Ottino, J. M. Monte Carlo Calculations of Cluster Statistics in Continuum Models of Composite Morphology. *J. Chem. Phys.* **1988**, *88*, 1198.
(58) Surve, M.; Pryamitsyn, V.; Ganesan, V. Polymer-Bridged Gels of Nanoparticles in Solutions of Adsorbing Polymers. *J. Chem. Phys.* **2006**, *22*, 969.
(59) Samanta, R.; Ganesan, V. Influence of dielectric inhomogeneities on the structure of charged nanoparticles in neutral polymer solutions. *Soft Matter* **2018**, *14*, 3748−3759.
(60) Fong, K. D.; Self, J.; Diederichsen, K. M.; Wood, B. M.; McCloskey, B. D.; Persson, K. A. Ion Transport and the True Transference Number in Nonaqueous Polyelectrolyte Solutions for Lithium Ion Batteries. *ACS Cent. Sci.* **2019**, *5*, 1250−1260.
(61) Zhu, L. Exploring strategies for high dielectric constant and low loss polymer dielectrics. *J. Phys. Chem. Lett.* **2014**, *5*, 3677−3687.
(62) Grzetic, D. J.; Delaney, K. T.; Fredrickson, G. H. The effective χ parameter in polarizable polymeric systems: One-loop perturbation theory and field-theoretic simulations. *J. Chem. Phys.* **2018**, *148*, 204903.

https://dx.doi.org/10.1021/acs.macromol.9b02510
Macromolecules 2020, 53, 875−884